CrossMark

A whole-brain computational modeling approach to explain the alterations in resting-state functional connectivity during progression of Alzheimer's disease

Murat Demirtaş[a,b,*], Carles Falcon[d,e], Alan Tucholka[d], Juan Domingo Gispert[d,e], José Luis Molinuevo[d], Gustavo Deco[a,c,f,g]

[a] Center for Brain and Cognition, Computational Neuroscience Group, Department of Information and Communication Technologies, Universitat Pompeu Fabra, Barcelona 08018, Spain
[b] Yale University, Psychiatry Department, New Haven, 06510, CT, United States
[c] Institució Catalana de la Recerca i Estudis Avançats (ICREA), Barcelona 08010, Spain
[d] Barcelonaβeta Brain Research Center, Pasqual Maragall Foundation, Barcelona, Spain
[e] Centro de Investigación Biomédica en Red de Bioingeniería, Biomateriales y Nanomedicina (CIBER-BBN), Zaragoza, Spain
[f] Department of Neuropsychology, Max Planck Institute for Human Cognitive and Brain Sciences, 04103 Leipzig, Germany
[g] School of Psychological Sciences, Monash University, Melbourne, Australia

ARTICLE INFO

ABSTRACT

Alzheimer's disease (AD) is the most common dementia with dramatic consequences. The research in structural and functional neuroimaging showed altered brain connectivity in AD. In this study, we investigated the whole-brain resting state functional connectivity (FC) of the subjects with preclinical Alzheimer's disease (PAD), mild cognitive impairment due to AD (MCI) and mild dementia due to Alzheimer's disease (AD), the impact of APOE4 carriership, as well as in relation to variations in core AD CSF biomarkers. The synchronization in the whole-brain was monotonously decreasing during the course of the disease progression. Furthermore, in AD patients we found widespread significant decreases in functional connectivity (FC) strengths particularly in the brain regions with high global connectivity. We employed a whole-brain computational modeling approach to study the mechanisms underlying these alterations. To characterize the causal interactions between brain regions, we estimated the effective connectivity (EC) in the model. We found that the significant EC differences in AD were primarily located in left temporal lobe. Then, we systematically manipulated the underlying dynamics of the model to investigate simulated changes in FC based on the healthy control subjects. Furthermore, we found distinct patterns involving CSF biomarkers of amyloid-beta (Aβ1 − 42) total tau (t-tau) and phosphorylated tau (p-tau). CSF Aβ1 − 42 was associated to the contrast between healthy control subjects and clinical groups. Nevertheless, tau CSF biomarkers were associated to the variability in whole-brain synchronization and sensory integration regions. These associations were robust across clinical groups, unlike the associations that were found for CSF Aβ1 − 42. APOE4 carriership showed no significant correlations with the connectivity measures.

1. Introduction

Alzheimer's disease (AD), being the most prevalent dementia, became a major concern in developed countries as a consequence of increasing life expectancy (Blennow et al., 2006; Plassman et al., 2007). During the past two decades advancements in genetics, neurobiology and neuroimaging techniques allowed researchers to study the mechanisms behind the underlying causes of AD. In particular, resting state functional Magnetic Resonance Imaging (rs-fMRI) became a widely used tool to study the alterations in brain activity of AD patients as well as many other clinical conditions (Greicius, 2008). Furthermore, cerebrospinal fluid (CSF) biomarkers have been shown to serve as a proxy to monitor in vivo the neuropathological hallmarks of AD, namely amyloid-β and tau tangles (José Luis Molinuevo et al., 2014).

Various rs-fMRI studies showed altered functional connectivity in AD (Brier et al., 2014; Dennis and Thompson, 2014; Filippi and Agosta, 2011). The studies that used seed-based approach showed widespread decreases in hippocampal (Allen et al., 2007; W. Li et al., 2012; Wang et al., 2006) and posterior cingulate functional connectivity (Bai et al., 2011; Zhang et al., 2009) in AD. In addition, some of these studies

reported increased FC between prefrontal cortex and hippocampus (Wang et al., 2006), and between prefrontal cortex and posterior cingulate (Bai et al., 2011; Zhang et al., 2009) in AD. The increased connectivity in prefrontal cortex was interpreted as a compensation mechanism during the initial stages of the disease (Dickerson et al., 2004; Filippi and Agosta, 2011; Sanz-Arigita et al., 2010). The studies based on independent component analysis (ICA) showed decreased activation of default mode network (DMN) (Agosta et al., 2012; Koch et al., 2010; Qi et al., 2010; Sorg et al., 2007) and increased activation of frontoparietal network (FPN) (Agosta et al., 2012). Various other studies found impaired deactivation of DMN during task in AD and dementia (Celone et al., 2006; Greicius et al., 2004; Lustig et al., 2003; Petrella et al., 2007; Rombouts et al., 2009, 2005).

Another powerful approach to study AD comprised the relationship between CSF biomarkers and the progression of AD. For example, amyloid-β plaques are known to accumulate decades before the onset of the first disease symptoms in individuals with prolonged phase of "preclinical AD" (Price and Morris, 1999). The analysis of CSF Aβ1 − 42 concentrations has been shown to closely correlate with cerebral pathology. Furthermore, to identify the functional manifestations of CSF biomarkers, rs-fMRI has been proposed as a promising approach (Barkhof et al., 2014). Several studies showed an overlap between the spatial pattern of the DMN and that of Aβ1–42 accumulation that happens in this preclinical phase of AD (Buckner et al., 2008; Hedden et al., 2009). Furthermore, DMN connectivity was decreased in cognitively normal individuals with augmented cerebral amyloid load (Sheline, Raichle, et al., 2010b; Hedden et al., 2009; Oh et al., 2011). In addition to Aβ1 − 42, altered functional connectivity in the DMN have also been associated to abnormal levels of phosphorylated Tau181 (p-tau) in CSF (Wang et al., 2013) as well as the ratio Aβ1–42/p-tau and the AD CSF Index (Jose Luis Molinuevo et al., 2013), both of which constitute well-established markers of disease progression (X. Li et al., 2013). Reduced DMN functional connectivity has also been reported in amyloid-free carriers of at least one copy of the APOE4 allele, which is the strongest genetic risk factor for AD (Sheline, Morris, et al., 2010a). These findings suggested that differences in functional connectivity might even precede amyloid deposition (Sheline and Raichle, 2013).

Despite robust findings addressing altered DMN connectivity in AD, the mechanisms behind this alteration are not clear. Furthermore, dysfunction of DMN is the most common finding in many other mental disorders (Broyd et al., 2009). Therefore, it is crucial to understand the relationship between structure, function and CSF biomarkers in AD (Ramirez et al., 2014; Filippi and Agosta, 2011).

In this study, we investigated the rs-FC alterations in preclinical Alzheimer's disease (PAD), mild cognitive impairment due to AD (MCI) and mild dementia due to Alzheimer's disease (AD). First, we studied the whole-brain connectivity in each group based on the fluctuations in global synchronization level between all brain regions. Then, to understand the role of distinct brain regions, we characterized the rs-FC of each region to the rest of the brain by adapting a previously employed technique to parcellated data (Cole et al., 2010). Moreover, we proposed whole-brain computational model to provide mechanistic understanding of the connectivity alterations in each group. We performed two experiments using the model: First, to understand the role of long-range interactions between regions on the rs-FC alterations in clinical groups, we estimated the effective connectivity in the model. Effective connectivity (EC) refers to the optimal connection strengths between the regions in the model that generate the observed FCs. Second, to test whether a global shift in the optimal dynamics explains the rs-FC alterations, we investigated the predicted changes in rs-FC by manipulating the model parameters in healthy control subjects (Fig. 1). Furthermore, we studied the association between core AD CSF biomarkers and described connectivity measures.

2. Materials and methods

2.1. Subjects

A total of 109 participants (58 HC, 12 PAD, 23 MCI and 16 AD) were recruited at the Alzheimer's disease and other cognitive disorders unit, from the Hospital Clinic of Barcelona. All subjects underwent clinical and neuropsychological assessment, MRI scanning and were submitted to a lumbar puncture to quantify the content of Aβ1–42, p-tau and t-tau in CSF. CSF biomarker quantitation was done at the local laboratory by means of ELISA (Enzyme-Linked ImmunoSorbent Assay kits, Innogenetics, Ghent, Belgium). An interdisciplinary clinical committee formed by two neurologists and one neuropsychologist established the diagnoses. HC and PAD presented no evidence of cognitive impairment on any of the administered neuropsychological tests, but PAD presented an abnormal level of CSF Aβ1–42 (below 500 pg/ml). MCI and AD presented signs of dementia. MCI patients had an objective memory deficit, defined as an abnormal score on the total recall measure of the Free and Cued Selective Reminding Test (FCRST) (over $1.5 \times$ standard deviation), impairment on one or more of the other cognitive tests or preserved activities of daily living, as measured by the Functional Activities Questionnaire (FAQ score $<$ 6). The NINCDS-ADRDA criteria were applied for probable AD diagnosis (Jack et al., 2011), taking into account clinical information and objective measures derived from the FAQ and neuropsychological results. AD patients were all in the mild stages of the disease (Global Deterioration Scale = 4). Diagnostic classification was made independent of CSF results. The local ethics committee approved the study and all participants gave written informed consent to participate in the study. Genomic DNA was extracted from peripheral blood of probands using the QIAamp DNA blood minikit (Qiagen AG, Basel, Switzerland). Apolipoprotein E genotyping was performed by polymerase chain reaction amplification and HhaI restriction enzyme digestion. Average demographic characteristics of the four diagnostic groups are shown in Table 1.

2.2. Image acquisition and preprocessing

Subjects were examined on a 3 T MRI scanner (Magnetom Trio Tim, Siemens, Erlangen, Germany) at the image core facilities of IDIBAPS (Barcelona, Spain). MRI session included a high-resolution three-dimensional structural T1-weighted image (sagittal MPRAGE; TR = 2300 ms, TE = 2.98 ms; matrix size = $256 \times 256 \times 240$; isometric voxel $1 \times 1 \times 1$ mm^3), a 10 min resting state fMRI (rs-fMRI; 300 volumes, TR = 2000 ms, TE = 16 ms, $128 \times 128 \times 40$ matrix, voxel size = $1.72 \times 1.72 \times 3$ mm^3) and two sets of diffusion weighted images (DWI; 30 no-collinear directions with a b value of 1000 s/mm^2 and one volume with a b value of 0; TR = 7700 ms, TE = 89 ms; matrix size = $122 \times 122 \times 60$; voxel size $2.05 \times 2.05 \times 2$ mm^3).

The pre-processing pipeline of rs-fMRI consisted in the slice-timing correction, the realignment and re-slice, smoothing with a Gaussian kernel (FWHM = 5 mm), second order de-trending and regressing out Volterra expanded parameters of movement (24 parameters), mean white matter (WM) signal, mean CSF signal and nulling regressors for bad volumes (Lemieux et al., 2007). Global signal regression (GSR) was not performed, because the known issues about GSR (Murphy et al., 2009) have a prominent impact on the analysis of whole-brain connectivity (Yang et al., 2014). Movement and other nuisance regressions were performed to alleviate the global artifacts. The quality criteria to consider a volume wrong and to override it by a nulling regressor, was that its correlation coefficient (cc) with the mean image of its series were beyond three standard deviations (cc $<$ 0.991) from the mean cc of all the images from all subjects to their corresponding mean image (mean cc = 0.995). No subjects presented $>$ 15% of bad volumes,
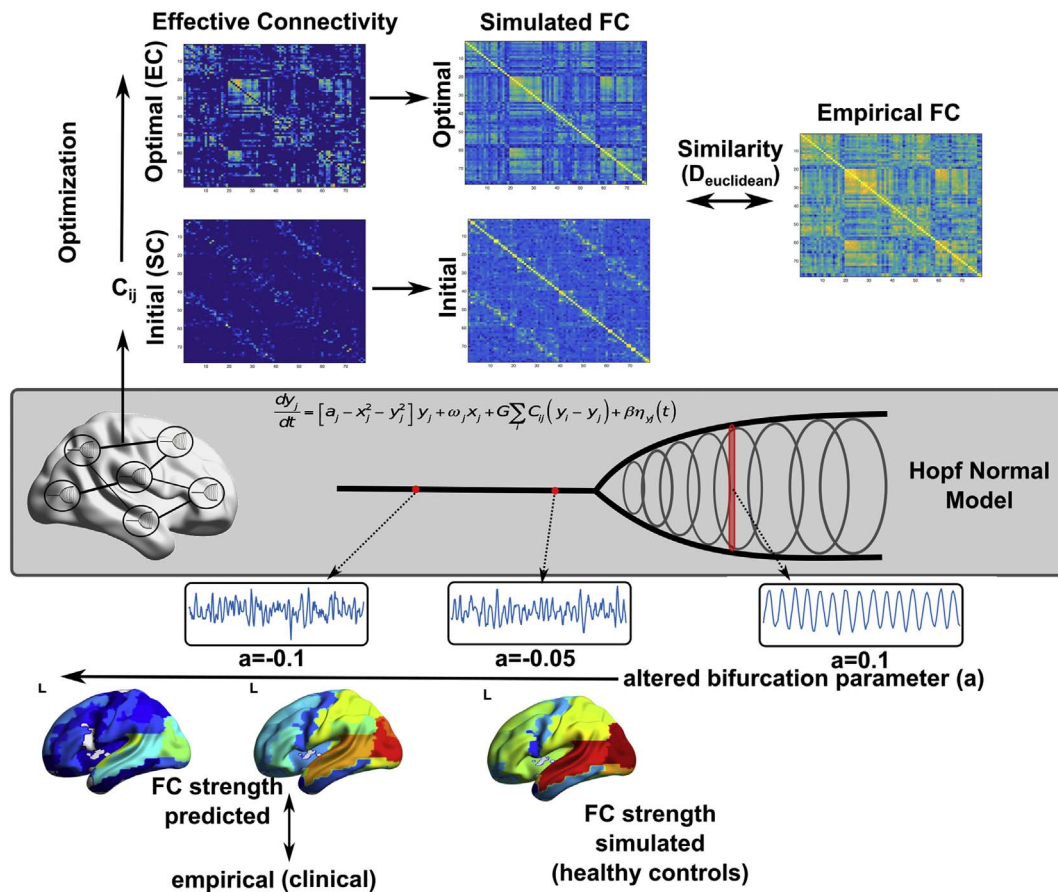
Fig. 1. Overview of the model. Top panel illustrates the optimization of the effective connectivity (EC). Middle panel illustrates Hopf normal model. Bottom panel illustrates the effect of local bifurcation parameter (a) and the overview of the computational experiment.

Table 1
Demographics.

	HC	PAD	MCI	AD
Age	60.72 (6.99)	69.00 (7.62)	69.73 (7.77)	65.00 (9.98)
Sex	37 (M), 20 (F)	9 (M), 3 (F)	14 (M), 9 (F)	9 (M), 7 (F)
APOE careers	0.15	0.42	0.52	0.50
CSF Biomarker Index	0.44 (0.26)	1.09 (0.55)	1.50 (0.42)	1.52 (0.43)
FR	27.23 (6.92)	21.25 (6.59)	8.95 (7.14)	6.23 (4.04)
TR	43.14 (4.44)	38.42 (7.06)	21.77 (12.95)	18.69 (12.48)
FDR	10.43 (2.34)	8.58 (3.18)	2.55 (3.20)	2.00 (2.52)
TDR	14.84 (1.26)	13.33 (2.46)	6.32 (5.25)	5.69 (4.87)

Key: AD, Alzheimer's Disease; HC, healthy controls; PAD, preclinical Alzheimer's disease; MCI, mild cognitive impairment; APOE, apolipoprotein E allele; CSF, cerebrospinal fluid; FR, free recall; TR, total recall; FDR, free differed recall; TDR, total differed recall.

being the average percentage of bad volumes of 1.6% and the standard deviation of 3.7%. To obtain the time series of each region from the Anatomical Automatic Labeling (AAL) atlas (Tzourio-Mazoyer et al., 2002), AAL atlas was adapted to every subject native space by co-registering it to the T1 structural image by mean of Advanced Normalization Tools (ANTs; UPENN, UVA and UIowa, USA; http://stnava.github.io/ANTs/). We kept the data in native space, because bringing the data to standard space slightly alters the data by interpolations. Moreover, we did not perform a voxel-wise analysis, which would require spatially normalized images. AAL maps in native space were resliced to fMRI resolution using nearest neighbor interpolation and masked with the gray mater (GM) mask. GM mask was constructed for every subject from the tissue probability maps resulted from segmentation of T1 images. The mask was formed by those voxels whose probability of belonging to GM was bigger than the probability of belonging to any other tissue. GM masks were dilated one voxel to include edges and to fill noise-related small gaps and, finally, resliced to fMRI resolution. Time series were obtained by averaging the fMRI signal in the each area of the GM-masked AAL atlas in native space (Tzourio-Mazoyer et al., 2002). The software used for the whole fMRI pre-processing, apart from the above mentioned ANTs, was a homemade MATLAB (Mathworks, Sherborn, MA, USA) scripts mostly formed by functions from SPM package (Wellcome Trust Center for Neuroimaging; UCL, UK; http://www.fil.ion.ucl.ac.uk/spm/).

DWI were first corrected for eddy current distortions using FMRIB Software Library (FSL) package (Jenkinson et al., 2012). Data was denoised using the overcomplete local principal component analysis (PCA) method described in (Manjón et al., 2013). Similarly, T1-weighted images were denoised using a non-local mean filter (Coupe et al., 2008) and then corrected for the usual acquisition bias with the N4 method from ANTs package (Tustison et al., 2010). Anatomical images were then segmented with VBM8 toolbox (Ashburner and Friston, 2000) to create GM, WM and CSF probabilistic maps. Bias-corrected T1 images were then co-registered to the non-gradient diffusion image and to the MNI template using ANT's (Avants et al., 2011). Brain regions from AAL template (Tzourio-Mazoyer et al., 2002) were then resampled to the diffusion space of each subject. Finally, FSL's Bedpostx and Probtrackx tractography was performed between AAL regions using default parameters. Cerebellum was not considered resulting in a 90 × 90 structural connectivity matrix.

2.3. Whole-brain connectivity measures

We quantified the measure of whole-brain connectivity based on level of synchronization in the BOLD time series of each group. Hilbert transform converts the narrowband signal as $a(t) = A(t)\cos(\varphi(t))$, where $A(t)$ is the instantaneous amplitude (or envelope), and $A(t)$, and $\varphi(t)$ is the instantaneous phase. The first and last 20 s (10 TR) of the transformed BOLD signal was then removed. The global coherence and metastability of the time-series were computed based on the Kuramoto Order Parameter (KOP) (Kuramoto, 1986; Shanahan, 2010; Cabral et al., 2012; Hellyer et al., 2014): $K(t) = \frac{1}{N} \sum_{j=1}^{N} \exp(i\varphi_j(t))$, where N is the number of ROIs and $\varphi(t)$ is the instantaneous phase of each region estimated using Hilbert Transform. The temporal average of Kuramoto Order Parameter defined as the coherence (mean synchronization), whereas the standard deviation of Kuramoto Order Parameter defined as the metastability (i.e. the variation in synchronization over time).

Since all the analyses relies on the choice of narrowband, to test the robustness of the proposed measures across frequency bands, we estimated the group differences in coherence and metastability in 7 narrowbands with 0.03 Hz bandwidth and frequency onsets varying between 0.01 Hz and 0.07 Hz (one-way ANOVA). We found significant group differences for both measures in frequency bands between onsets of 0.03 and 0.07 (i.e. 0.03–0.07 Hz to 0.07–0.1 Hz). The differences were significant except 0.01–0.04 Hz narrowband (Supplementary Fig. 1). Due to high computational demand of the modeling framework, for the rest of the analyses we focused on 0.06–0.09 Hz narrowband in which the group differences were high for both coherence and metastability. Furthermore, the 0.06 Hz frequency onset is also consistent with a previous study that showed the highest discriminative power for classification of MCI and AD was achieved between 0.054 and 0.068 Hz range (Wee et al., 2012). An alternative approach to define the narrowband would be to choose 0.04–0.07 Hz range, in which the BOLD signal is relatively less affected by known artifacts (Glerean et al., 2012). We repeated the group comparison and CSF biomarker correlation analyses based on whole-brain and FC (Supplementary Fig. 2–3). Most of the results remained unchanged when 0.04–0.07 Hz narrowband was used with some exceptions: group differences in coherence was insignificant after regressing out age, group differences in FC between AD-HC were more symmetric across hemispheres (Supplementary Fig. 2), and CSF biomarker correlations were absent in right prefrontal cortex (Supplementary Fig. 3).

The FC was computed as the Pearson's correlation between the time-series of different brain regions. Then, as a measure of regional connectivity, we used functional connectivity (FC) strength, which was calculated as the sum of FCs of each region to the rest of the regions. Previously global brain connectivity (GBC) was proposed to measure the regional variations in FC (Cole et al., 2010). Here, we preferred the term FC strength, used in graph theory, to emphasize that the measure was based on parcelled data.

2.4. Computational model

We modeled the whole-brain rs-fMRI BOLD signals using 78 nodes, excluding subcortical regions. The role of subcortical regions in whole-brain computational models is not well studied and subcortical regions are often excluded in these studies. The list of the regions and abbreviations were provided in Supplementary Table 1. Each node was coupled with each other via effective connectivity (EC) matrix. We described the local dynamics of each individual node using normal form of a supercritical Hopf bifurcation. The advantage of this model is that it allows transitions between asynchronous noise activity and oscillations. Where ω is the intrinsic frequency of each node, a is the local bifurcation parameter, η is additive Gaussian noise with standard deviation β, the temporal evolution of the activity, z, in node j is given in complex domain as:

$$\frac{dz_j}{dt} = [a_j + i\omega_j - |z_j^2|] + \beta\eta_j(t)$$

and,

$$z_j = \rho_j e^{i\theta_j} = x_j + iy_j$$

This system shows a supercritical bifurcation at $a_j = 0$. Being specific, if a_j is smaller than 0, the local dynamics has a stable fixed point at $z_j = 0$, and for a_j values larger than 0, there exists a stable limit cycle oscillation with a frequency $f = \omega/2\pi$. Finally, the whole-brain dynamics is described by the following coupled equations:

$$\frac{dx_j}{dt} = [a_j - x_j^2 - y_j^2]x_j - \omega_j y_j + G \sum_i C_{ij}(x_i - x_j) + \beta\eta_{xj}(t)$$

$$\frac{dy_j}{dt} = [a_j - x_j^2 - y_j^2]y_j + \omega_j x_j + G \sum_i C_{ij}(y_i - y_j) + \beta\eta_{yj}(t)$$

where C_{ij} is the Effective Connectivity (EC) between nodes i and j, G is the global coupling factor, and the standard deviation of Gaussian noise, $\beta = 0.02$. The natural frequency (f) of each region was taken as the peak frequency in the given narrowband of the corresponding region in the empirical time-series. The simulated activity corresponds to the BOLD signal of each node. The simulations were run for 30,000 s, sampled at 2 s, if not stated otherwise. Both the empirical and simulated BOLD signals were band-pass filtered in narrowband 0.06–0.09 Hz, since the group differences in coherence and metastability were optimal in this narrowband. The intrinsic frequency of each node was estimated as the peak frequency in the associated narrowband of the empirical BOLD signals of each brain region.

2.5. Optimization of effective connectivity

We implemented a heuristic approach to infer the most likely connectivity matrix (i.e. Effective Connectivity) that maximizes the similarity between empirical and simulated functional connectivity. As an initial guess, we used DWI-derived structural connectivity matrices (Fig. 1). First, we adjusted the global coupling parameter (G) to prevent overflow during the optimization procedure, and to ensure the stability of the system of equations. Where K^{sim} and K^{emp} are simulated and empirical coherences (average Kuramoto order parameter), we updated global coupling parameter as: $G = G \exp(K^{sim} - K^{emp})$, until the desired condition, $|K^{sim} - K^{emp}| < 0.1$, was satisfied.

We evaluated both zero-time-lag Functional Connectivity (FC⁰) and time-lagged FC (FCᵗ) for both empirical and simulated BOLD signals. Time-lagged FC measure was chosen for two reasons. First, it provides an additional constraint ensuring that the optimal solution is unique. Second, time-lagged correlations allow inference on the directionality of the connections. The defined the distance metric as Euclidean Distance between simulated and empirical FC values for both FC⁰ and FCᵗ:

$$D^l = \sqrt{\sum_{i,j=1}^{N} (FC_{ij}^{sim,l} - FC_{ij}^{emp,l})^2}, \, l \in \{0, \tau\}$$

Then, where E is the average error between empirical and simulated FC measures;

$$E = \frac{(F_{emp}^0 - FC_{sim}^0) + (FC_{emp}^\tau - FC_{sim}^\tau)}{2}$$

where S_{ij} is the anatomical connectivity matrix, N is the number of regions, and Λ denoted inter-hemispheric links; we updated the effective connectivity between i and j = (1, …, N) according to: $C_{ij}^{update} = C_{ij}^{current} + 0.01E_{ij}$, if $S_{ij} > 0$, or $S_{ij} \in \{\Lambda\}$ $C_{ij}^{update} = 0$, if $S_{ij} = 0$, or $C_{ij}^{current} + 0.01E_{ij} < 0$

In other words, we updated the EC based on the average error between empirical and simulated FC measures for non-zero connections and inter-hemispheric connections. Negative weights were not allowed, and they all set to zero during the update procedure.

We accepted the total distance between empirical and simulated FC measures, $D^T = D^0 + D^\tau$, for updated EC is lower than the minimum total distance observed during the procedure. We repeated this procedure using 100 iterations, and the best solution (minimum D) was considered as EC for a given subject. The entire procedure was also repeated for bifurcation parameter $a = \{-0.1, -0.05, 0, 0.05, 1\}$. The best fit for the majority of the subjects was achieved at a = − 0.05 (Supplementary Fig. 4A). For consistency, we fixed the bifurcation parameter at a = − 0.05 for all the subjects. Finally, the EC strengths were computed as the sum of input and output weights of each node.

2.6. Computational experiment

Given the inferred EC matrices, we disrupted the dynamics in healthy controls based on the bifurcation parameter (a) of the supercritical Hopf Normal Model (Fig. 1). In brief, the local bifurcation parameter characterizes whether the underlying dynamics of each node are primarily asynchronous (a < 0) or oscillatory (a > 0). The model was discussed in detail in a recent paper (Deco et al., 2017). First, we computed the FC of the healthy controls at a = − 0.05, where the optimal similarity between simulated and empirical values was observed. Then, we decreased the bifurcation parameter by 0.001 at each iteration, spanning values between − 0.05 and − 0.15. The FC strengths (FC^a) were computed for each *a*. Then, the distance between the average FC strength at each bifurcation parameter and the group averaged empirical FC strength for each clinical group (PAD, MCI, AD) was calculated. The distance was quantified as Euclidean distance between predicted and empirical FC. Finally, we used principal component analysis to investigate the main effects on FC strength across manipulated bifurcation parameters.

2.7. Statistical analyses

The group comparisons (for coherence, metastability, FC strength, EC strength) were done using permutation *t*-test (10,000 permutations), and multiple comparisons were corrected using FDR approach with Benjamini & Hochberg algorithm if necessary (Hochberg and Benjamini, 1990). Prior to group comparisons, we regressed out subject's age from each measure. The networks were visualized using BrainNet Viewer toolbox in Matlab (Xia et al., 2013). Correlations between CSF biomarkers (APOE-4, Aβ-42, t-tau and p-tau) and the measures (coherence, metastability, FC strength, EC strength) were estimated as the partial correlations controlled for age, gender and education level. APOE was quantified as the carriers and non-carriers of the gene.

3. Results

3.1. Whole-brain connectivity

We characterized the whole-brain connectivity of each group using mean (coherence) and standard deviation (metastability) of Kuramoto order parameter, which quantifies the level of synchronization between brain regions across time. We found significant correlations between diagnostic category and coherence ($r = -0.37$, *p*-value < 0.01), and metastability ($r = -0.33$, *p*-value < 0.01). After regressing out age as confounding variable, we compared coherence and metastability across HC, PAD, MCI, and AD groups using permutation *t*-test (10,000 permutations, *p*-value < 0.05). The coherence and metastability in the AD group were significantly lower than those in HC group (coherence: T-statistic = 3.4, *p*-value < 0.01; metastability: T-statistic = 3.27, *p*-value < 0.01) and those in PAD group (coherence: T-statistic = 2.77, *p*-value < 0.05; metastability: T-statistic = 2.84, *p*-value < 0.01) (Fig. 2A–B). We found no significant differences in coherence and metastability across the rest of the groups (Supplementary Table 2). These results showed that the magnitude and variability of whole-brain connectivity is decreasing along with the progression of the disease, which reaches statistical significance in AD.
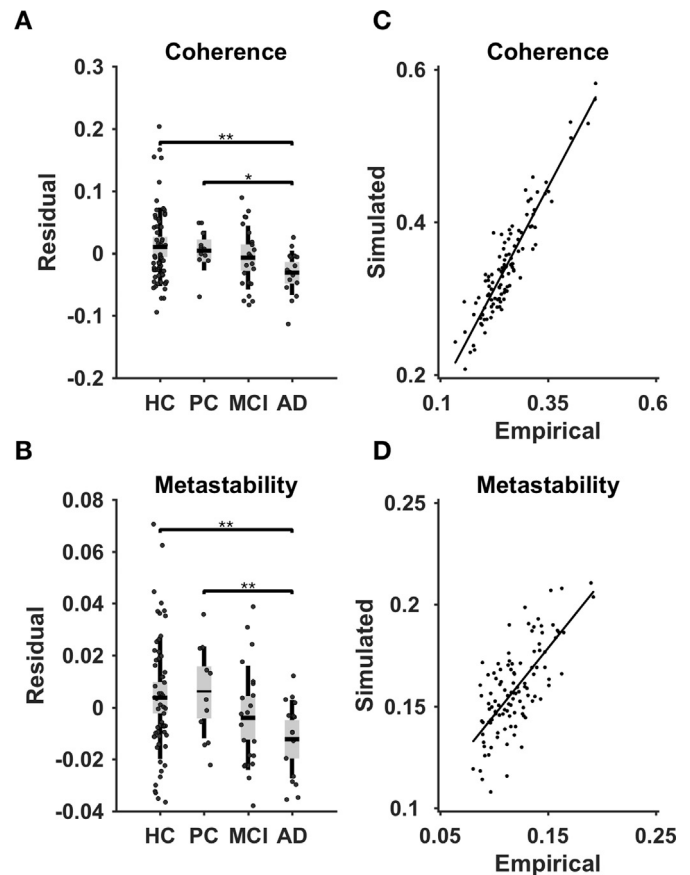

Fig. 2. A Group differences in coherence (average Kuramoto order parameter). B Group differences in metastability (standard deviation of Kuramoto order parameter). The results are shown for 0.06–0.09 Hz narrowband signal. The comparisons were done using permutation *t*-test (10,000 permuations; *p < 0.05, **p < 0.01) after regressing out age as a confounding variable. C The correspondence between empirical and simulated coherence. D The correspondence between empirical and simulated metastability.

3.2. Computational model

We proposed a whole-brain computational approach to model the whole-brain connectivity of each subject. Based on the similarity between empirical and simulated FC, we estimated the effective connectivity (EC) between brain regions. The average correlation coefficient between empirical and simulated FC was $r = 0.81$ (std = 0.03). Furthermore, the correlation coefficients between empirical and simulated coherence and metastability were $r = 0.93$ (*p*-value < 0.001) and $r = 0.72$ (*p*-value < 0.001), respectively (Fig. 2C–D). Therefore, the proposed model not only showed high similarity to the empirical FC, but also accounted for the variations in coherence and metastability.

3.3. Regional connectivity

To investigate the regional variations in whole-brain connectivity, we compared the strengths of functional connectivity (FC) and strengths of effective connectivity (EC) of PAD, MCI and AD groups with those of HC group. AD group exhibited significantly decreased FC strengths widespread across the cortex (Fig. 3A) (Table 2). No significant differences were found in FC strengths of PAD and MCI groups. In contrast, significant decreases in EC strengths were located in left temporal lobe in AD group (Fig. 3B). Furthermore, EC strengths in PAD group were significantly decreased in left-precentral gyrus (T-statistic = 2.82, FDR adjusted *p*-value < 0.05), left hippocampus (T-statistic = 3.88, FDR adjusted *p*-value < 0.05) and right temporal pole
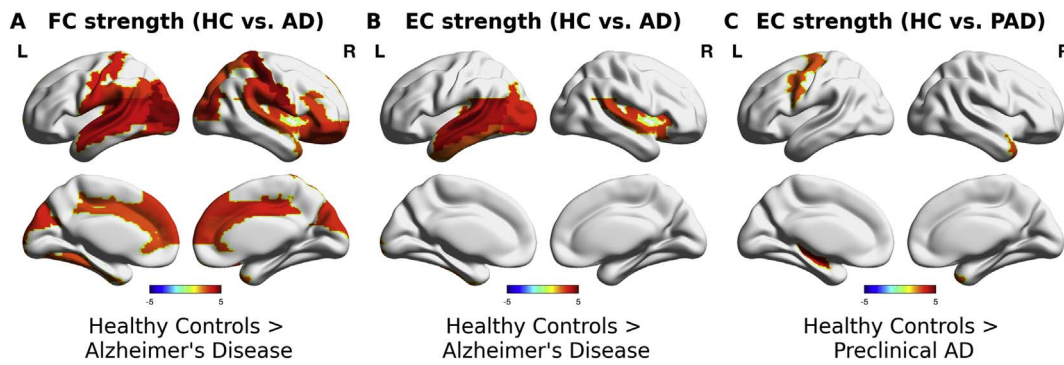
Fig. 3. Group differences in FC and EC strengths. A FC strength of healthy control group vs. Alzheimer's disease (AD) group. B EC strength of healthy control group vs. Alzheimer's disease (AD) group. C EC strength of healthy control group vs. preclinical Alzheimer's disease subjects (PAD). The comparisons were done using permutation *t*-test (10,000 permuations) after regressing out age as a confounding variable. Colorbars indicate T-statistic, where hot colors indicate higher values in healthy control group. Only the regions that showed significant differences after FDR correction (adjusted *p*-value < 0.05) were shown.

Table 2
Significant differences in FC and EC strengths.

FC Strength	(HC vs. AD)	EC Strength	(HC vs. AD)
ROI	T-statistic	ROI	T-statistic
l-MOG	4.6237	l-MTG	4.2007
r-PoCG	4.5427	l-IOG	3.9683
l-STG	4.0204	l-STG	3.5094
l-MTG	3.9036	l-HES	3.4922
l-HES	3.7915	l-MOG	3.3404
l-IOG	3.6295	r-INS	3.2251
l-PoCG	3.5312	r-STG	3.0947
r-MOG	3.5258	l-ITG	2.7366
l-ROL	3.4757	EC Strength	(HC vs. PC)
r-DCG	3.4686	ROI	T-Statistic
l-CUN	3.4414	l-HIP	3.8781
r-ROL	3.4013	r-TPOmid	2.9248
r-SMG	3.3754	l-PreCG	2.8196
r-ORBinf	3.3300		
r-SFGmed	3.3281		
r-ORBmid	3.3205		
l-SOG	3.3086		
r-CUN	3.2861		
r-ORBsup	3.2579		
r-INS	3.2364		
l-SMG	3.2118		
l-SFGmed	3.1908		
l-ANG	3.1634		
r-ACG	3.1387		
r-IFGtriang	3.0819		
r-STG	3.0325		
r-SOG	3.0077		
l-FFG	2.9761		
l-DCG	2.9755		
r-SPG	2.8759		
l-ACG	2.8703		
r-TPOmid	2.8015		

FDR-adjusted *p*-values < 0.05.

(T-statistic = 2.92, FDR adjusted *p*-value < 0.05) (Fig. 3C). No significant differences were found in MCI group. These results showed that the model-based estimate of EC restricted the regional alterations to the left temporal lobe.

3.4. APOE4 and CSF biomarkers

We investigated the relationship between whole-brain/regional connectivity and APOE4 allele carrier status and CSF biomarkers. We calculated the partial correlations between each whole-brain/regional connectivity measure and APOE4 carrier status and CSF biomarkers (Aβ1–42, t-tau, p-tau) controlling for age, gender and education level. We performed the analysis across clinical groups (i.e. PAD, MCI, and AD

subjects) and across all subjects (i.e. HC, PAD, MCI and AD subjects), separately.

Regarding the whole-brain connectivity measures, APOE4 allele carrier status showed no significant correlations with coherence and metastability (Table 3). Across all subjects, coherence showed a significant correlation with Aβ1–42 (rho = 0.23, *p*-value < 0.05). However, across clinical groups there were no significant correlations between Aβ1–42 and coherence (Table 3). Coherence showed no significant correlations with t-tau and p-tau (Table 3). In contrast, we found no correlations between metastability and Aβ1–42. Metastability was significantly correlated with t-tau (across all subjects, rho = − 0.27, *p*-value < 0.01; across clinical groups, rho = − 0.31, *p*-value < 0.05) and p-tau (across all subjects, rho = − 0.27, *p*-value < 0.01; across clinical groups, rho = − 0.36, *p*-value < 0.05) (Table 3). These results showed that Aβ1–42 CSF levels reflect the attenuation in coherence (average synchronization) due to its prevalence, but these levels do not correlate with the progression of AD. In contrast, the correlations between t-tau/p-tau CSF biomarkers and metastability (variability in synchronization) are also consistent with the progression of AD.

Across all subjects, CSF Aβ1–42 showed significant positive correlations with FC strength and EC strength (Fig. 4A–B) (Table 4). The spatial maps of these correlations were highly overlapping with the group differences between AD and HC subjects (Fig. 4A–B). For p-tau and t-tau CSF biomarkers, we found significant negative correlations with FC strengths in frontal, parietal and occipital regions, and with EC strengths in occipital and parietal regions (Fig. 4C–E) (Table 5). Across clinical groups, CSF Aβ1–42 showed no positive correlations with FC and EC strengths. In contrast, we found significant negative correlations between CSF Aβ1–42 and left orbital frontal FC strength (rho = − 0.38,

Table 3
Partial correlations (rho) between CSF biomarkers and whole-brain connectivity measures.

	Across all subjects			
	APOE-4 allelle carrier status	Aβ-42	t-tau	p-tau
Coherence	− 0.1264	0.2343*	− 0.1221	− 0.1307
Metastability	− 0.0631	0.1349	− 0.2664**	− 0.2738**

	Across clinical groups			
	APOE-4 allelle carrier status	Aβ-42	t-tau	p-tau
Coherence	− 0.0398	− 0.0004	− 0.0079	− 0.0965
Metastability	− 0.019	0.0207	− 0.3097*	− 0.3647*

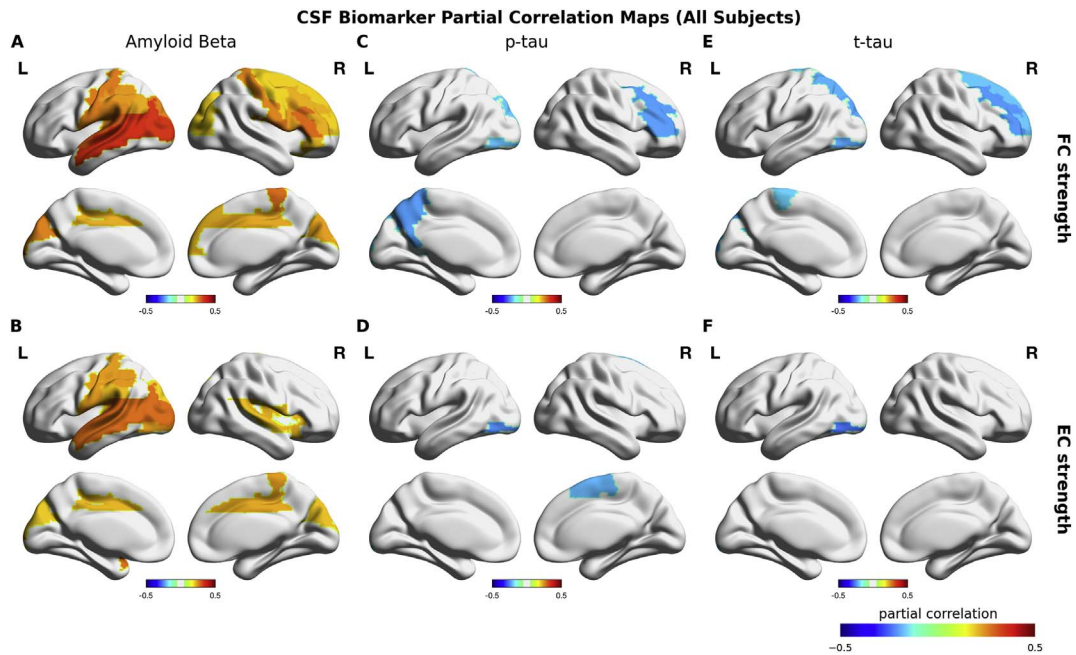* *p*-value < 0.05.
** *p*-value < 0.01.

Fig. 4. CSF biomarker partial correlation maps across all subjects. Upper row shows the relationship between FC strength and each CSF biomarker. Bottom row shows the relationship between EC strength and each CSF biomarker. Colorbars indicate the partial correlation coefficient (rho) between Aβ-42 and FC (A), between Aβ-42 and EC (B), between p-tau and FC (C), between p-tau and EC (D), between t-tau and FC (E), between t-tau and EC (F) that were calculated across all subjects controlled for age, gender and education level. Only significant correlations were colored on cortical surface plots.

We found similar trends in regional connectivity measures (FC and EC strengths) (this figure and Fig. 5) (Supplementary Tables 3–6). We found no significant correlations between APOE4 allele carrier status and FC strengths (across all subjects and across clinical groups) and EC strengths (across all subjects). Across clinical groups, left superior frontal EC strength showed a significant correlation with APOE-4 allele carrier status (rho = − 0.30, p-value < 0.05) (Supplementary Tables 3–6).

Table 4
Partial correlations between Aβ-42 CSF biomarker and FC-EC strengths.

FC strength		EC strength	
ROI	rho	ROI	rho
l-MTG	0.3402**	l-STG	0.2887**
l-MOG	0.3293**	l-MTG	0.2785**
l-STG	0.2946**	l-MOG	0.2773**
r-IFGtriang	0.2817**	l-TPOsup	0.2759**
r-PCL	0.2789**	l-ROL	0.2528**
r-ROL	0.2682**	l-IPL	0.2435*
l-PoCG	0.2664**	l-IOG	0.2409*
l-CUN	0.2615**	l-PoCG	0.2405*
l-SOG	0.2594**	r-PCL	0.2400*
r-PoCG	0.2574**	r-DCG	0.2301*
l-SMG	0.2545**	r-INS	0.2225*
l-ROL	0.2538**	r-ROL	0.2210*
l-HES	0.2502**	l-DCG	0.2191*
l-IPL	0.2411*	r-STG	0.2150*
r-IFGoperc	0.2380*	l-SMG	0.2137*
r-CUN	0.2358*	r-CUN	0.2109*
r-DCG	0.2304*	l-HES	0.2061*
l-ANG	0.2284*	l-CUN	0.2053*
r-MFG	0.2257*	l-SOG	0.1982*
l-DCG	0.2252*		
r-SFGmed	0.2195*		
r-ORBinf	0.2183*		
r-SFGfor	0.1991*		
r-MOG	0.1981*		
r-SOG	0.1973*		
r-PreCG	0.1971*		

 * p-value < 0.05.
** p-value < 0.01.

Table 5
Partial correlations between t-tau and p-tau CSF biomarkers and FC-EC strengths.

ROI	FC strength			
	Across all subjects		Across clinical groups	
	t-tau	p-tau	t-tau	p-tau
l-SOG	− 0.2282*	− 0.2011*	− 0.2944*	− 0.3287*
l-IOG	− 0.2264*	− 0.2045*	− 0.4215**	− 0.4529**
l-SPG	− 0.2187*	− 0.188	− 0.3371*	− 0.3730*
l-PCL	− 0.1946*	− 0.1473	− 0.2451	− 0.2146
r-SFGfor	− 0.2005*	− 0.1928	− 0.1437	− 0.1788
r-MFG	− 0.2359*	− 0.2322*	− 0.199	− 0.2253
r-IFGtriang	− 0.1744	− 0.2309*	− 0.1101	− 0.2818
l-PCUN	− 0.1865	− 0.2320*	− 0.1773	− 0.2869
r-ITG	− 0.1626	− 0.1079	− 0.3212*	− 0.276
l-IPL	− 0.1891	− 0.1566	− 0.2615	− 0.2935*
l-DCG	− 0.0236	− 0.0268	0.3080*	0.2415
r-OLF	0.0597	0.0399	0.2894	0.3082*

ROI	EC strength			
	Across all subjects		Across clinical groups	
	t-tau	p-tau	t-tau	p-tau
l-IOG	− 0.2638**	− 0.2438*	− 0.3817**	− 0.4382**
r-SMA	− 0.1903	− 0.2124*	− 0.2237	− 0.3048*
l-SOG	− 0.1557	− 0.1605	− 0.2364	− 0.2986*

 * p-value < 0.05.
** p-value < 0.01.

subjects (Fig. 5C–E). In particular, superior parietal gyrus, superior and inferior occipital gyri in left hemisphere were the most consistent regions and the magnitude of the correlations in these regions were substantially higher across clinical than those across all subjects (Table 5). Furthermore, FC strength showed significant positive correlations between t-tau CSF biomarker in left dorsal cingulate and between CSF p-tau in right olfactory cortex (Table 5). The results suggested distinct roles of Aβ1–42 and tau CSF biomarkers in AD.

p-value < 0.01) and EC strength (rho = − 0.30, p-value < 0.05), and right rectus EC strength (r = − 0.31, p-value < 0.05) (Fig. 5A–B). The spatial maps of the correlations of p-tau and t-tau CSF biomarkers were relatively consistent across clinical groups with those found across all

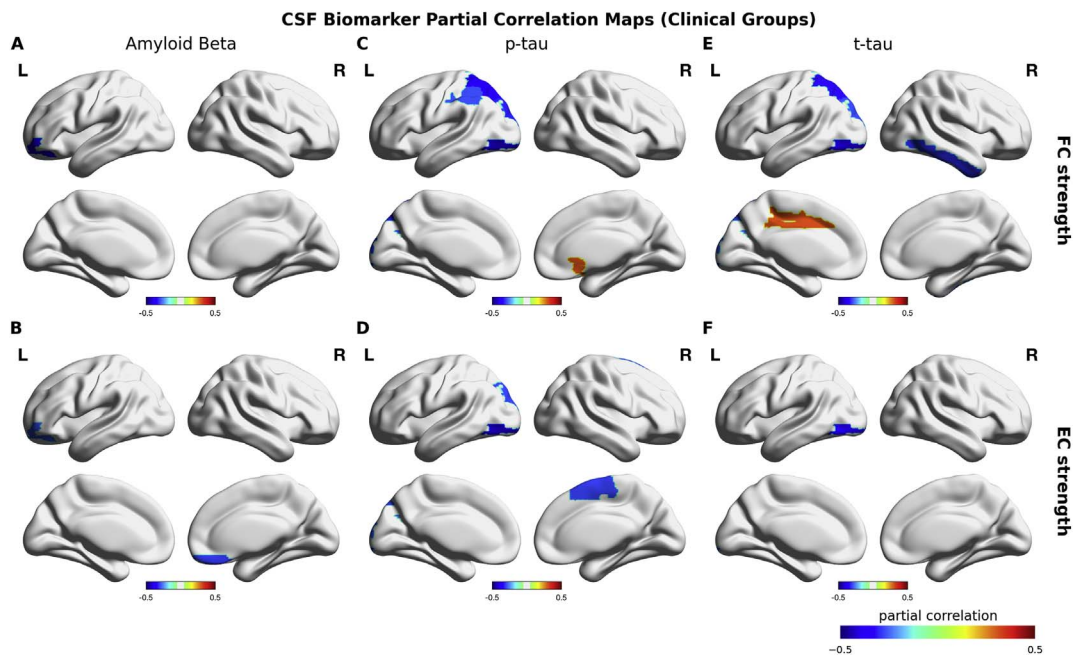**CSF Biomarker Partial Correlation Maps (Clinical Groups)**

Fig. 5. CSF biomarker partial correlation maps across clinical groups. Upper row shows the relationship between FC strength and each CSF biomarker. Bottom row shows the relationship between FC strength and each CSF biomarker. Colorbars indicate the partial correlation coefficient (rho) between Aβ-42 and FC (A), between Aβ-42 and EC (B), between p-tau and FC (C), between p-tau and EC (D), between t-tau and FC (E), between t-tau and EC (F) that were calculated across PC, MCI and AD groups controlled for age, gender and education level. Only significant correlations were colored on cortical surface plots.

3.5. Computational experiment

To link the altered whole-brain and regional connectivity, we conducted a computational experiment. Based on the proposed model, we systematically manipulated the local bifurcation parameter (a) in healthy control subjects to characterize the alterations in whole-brain and regional connectivity due to a global shift in optimal dynamics. Being specific, we disrupted the local dynamics of all regions in favor of noisy dynamics in healthy control subjects and checked the effects of this manipulation on simulated FC strengths. We found that the Euclidean distances between empirical FC strengths of each clinical group (PAD, MCI and AD) and predicted FC strengths were minimized at distinct bifurcation parameter values consistent with the hypothesis that the divergence from optimal dynamics aligns with the progression of AD (Fig. 6A). Furthermore, coherence and metastability at the predicted bifurcation parameter values were consistent with the empirically observed values in each clinical group (Fig. 6B–C). We used principal component analysis (PCA) on predicted FC strengths along the manipulated bifurcation parameter. Then, we extracted the spatial map based on the factor weights (scores) of the first principal component (PC) reflecting the main effect of the manipulation with 85% of the explained variance (Fig. 7A–B). We found that the spatial map of the first PC was correlated with the FC strengths of HC group ($r = 0.97$, p-value < 0.001). Furthermore, the spatial map of the first PC showed significant correlations with those of CSF biomarkers and cognitive performance scores (Fig. 7C). These results showed that the attenuation of the FC strength in each region is proportional to its initial magnitude. Furthermore, the empirically observed alterations in FC strengths primarily reflect these proportional attenuations due to the disintegration of the whole-brain connectivity.

4. Discussion

In this paper, we studied the changes in whole-brain and regional connectivity in PAD, MCI and AD. We treated the condition as a *continuum* based on severity comprising PAD, MCI and AD. We found that the whole-brain connectivity decreased through the *continuum* reaching

significance only in AD group. Decreased whole-brain synchronization was also reported recently in AD (Córdova-Palomera et al., 2017). The alterations in regional connectivity were also consistent with this trend. We proposed a whole-brain computational model to explore the mechanisms behind these alterations.

We showed that the strongly connected brain regions were affected more severely than other brain regions. Confirming the previous findings on FC impairments in AD, these regions were overlapping with default mode network (DMN). However, alterations in DMN were also reported in many other mental disorders (Broyd et al., 2009). This is an expected result, because the regions forming DMN repeatedly found as the structural hubs of the brain (Hagmann et al., 2008; Margulies et al., 2016). We hypothesized that the core alterations in connectivity might be obscured in FC due to the propagation of impaired activity. To reveal the connectivity changes in a deeper level, we used model-based inference of effective connectivity (EC). Although these two measures are related as one is derived from the other, they are not equivalent. First, unlike FC, EC is explicitly constrained by the anatomical connectivity. Second, in FC the contribution of direct and indirect connections between brain regions is unknown, whereas EC seeks the optimal configuration in which the direct connections sufficiently explain FC. It is important to note that in this study EC inference does not rely on generative models of underlying neural activity (Friston et al., 2003) or statistical models (Rogers et al., 2010). Instead, we defined EC as the parameter space optimized for the given dynamical system that lumps together various biophysical features of the underlying neural activity as well as hemodynamic properties of observed BOLD signal. Confirming our hypothesis, we found decreased EC strength in AD primarily affecting left temporal lobe, as opposed to the widespread decreases in FC strength. These results are more consistent with the previous findings on the spatial distribution and the lateralization in early stages of AD (Thompson et al., 2003; Singh et al., 2006). We did not find significant FC differences in PAD and MCI groups. PAD subjects exhibited decreased EC strength in several regions including the left hippocampus, whereas no significant EC differences were found in the MCI group. Previous studies reported mixed results regarding FC alterations in the early stages of the disease. These results were often
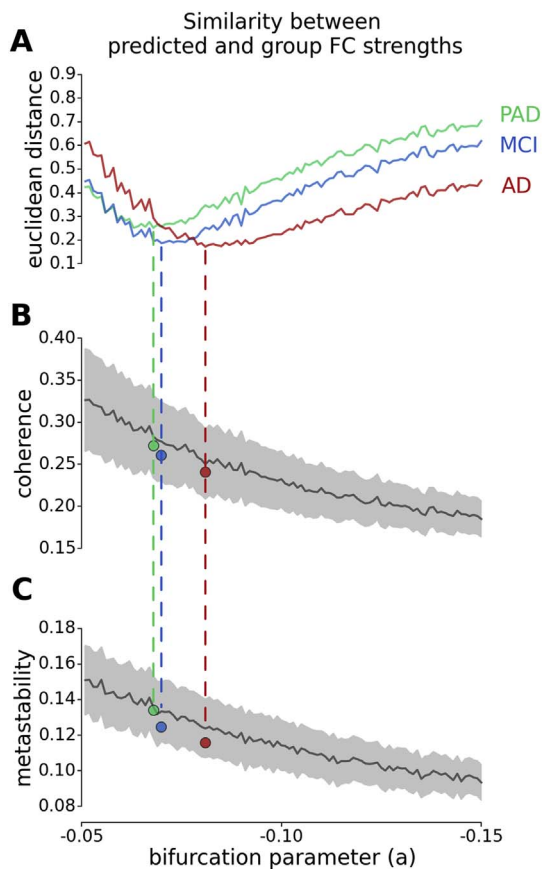
A Similarity between predicted and group FC strengths

Fig. 6. Computational experiment. FC strengths were calculated after performing simulations with manipulated local bifurcation parameters (within range − 0.05 and − 0.15) based on healthy control subjects. A The Euclidean distance between simulated FC strengths and group averaged empirical FC strengths of PAD (green), MCI (blue) and AD (red) subjects. Dashed lines indicate the minimum distance between simulated FC strengths and group averaged empirical FC strengths of each group, colored accordingly. B The simulated coherence with respect to manipulated local bifurcation parameters. C The simulated metastability with respect to manipulated local bifurcation parameters. Gray shadings show the standard deviations of each parameter across subjects. Colored dots indicate the average empirical coherence and metastability of PAD (green), MCI (blue) and AD (red) groups. (For interpretation of the references to color in this figure legend, the reader is referred to the web version of this article.)

interpreted as a compensation mechanism to maintain cognitive function under the pathology related insults in the preclinical stage of AD (Dickerson et al., 2004; Filippi and Agosta, 2011; Sanz-Arigita et al., 2010). When the brain cannot compensate any longer, cognition levels cannot be sustained and decline below normal ranges.

We confirmed the relationship between whole-brain and regional connectivity by conducting a computational experiment. Based on the inferred EC in healthy control subjects, we calculated the changes in FC strength with manipulated the local bifurcation parameters. Being specific, we systematically diverged dynamical system from the bifurcation point such that each node exhibited noise-driven dynamics and the functional integration was disrupted. The severity of the predicted decrease in FC strength of each node was determined by its FC strength at the origin. This result demonstrated that the connectivity hubs in the brain are more vulnerable to the perturbations in local dynamics. The spatial patterns associated to the perturbations were also correlated with those associated to the CSF biomarkers. Furthermore, the bifurcation parameter maximizing the similarity between predicted and observed FC strengths of each clinical group was consistent with the diagnosis (i.e. divergence from optimal bifurcation parameter was higher in AD than in MCI, and higher in MCI than in PAD). These findings support the view that abnormal synchronization in neural

circuits may underlie the development of clinical symptoms in AD (Palop and Mucke, 2016). An unexpected prediction of the computational model was the emergence of spatially structured increases in FC strengths for slight deviations in bifurcation parameter (Supplementary Fig. 9). A rapid decrease in variance of the hub regions might be responsible for these FC increases, which were prominent in cingulate cortex and precuneus in right hemisphere. Future studies are needed to investigate counter-intuitive network effects that are critical to interpret FC alterations.

We also investigated the role of genetic and CSF biomarkers during the progression of AD. We found distinct patterns for Aβ1–42 and tau CSF biomarkers. The correlations between CSF Aβ1–42 and whole-brain/regional connectivity were dramatically different across clinical groups than those found across all subjects. Across all subjects, CSF Aβ1–42 showed significant correlations with coherence (average synchronization) and FC strengths of the regions that were altered in AD. Furthermore, the correlations between CSF Aβ1–42 and whole-brain/regional connectivity were not present across clinical groups. These results are consistent with the findings that amyloid-β was associated with abnormal DMN connectivity in elders without dementia (Sheline, Raichle, et al., 2010b; Sperling et al., 2009). These findings also support the previous studies, which showed that cortical amyloid load is correlated with cognitive function in healthy individuals, but this relationship was absent in AD (Pike et al., 2007). Furthermore, disruption of the correlations across clinical groups supports the findings that Aβ1–42 is more relevant to the presence of connectivity alterations, but not the progression of the symptoms (Musiek and Holtzman, 2015).

In contrast, t-tau and p-tau CSF biomarkers were correlated with metastability (variability in synchronization) both across all subjects and across clinical groups. This finding also support the idea that metastability might be a more robust measure of functional integration in the brain (Deco and Kringelbach, 2014). Furthermore, tau CSF biomarkers were significantly correlated with FC/EC strengths in posterior and occipital brain regions. The regional correlation maps of CSF biomarkers were consistent with those of PET tau and Aβ topographies (Brier et al., 2016). Similar to the correlations with metastability, t-tau and p-tau correlations across clinical groups were relatively more consistent than Aβ1–42. The spatial patterns of these correlations were much more consistent in EC that those in FC. These results supported the findings that tau is a stronger predictor of cognition than Aβ (Brier et al., 2016). In addition, previous studies suggested that the impact of amyloid-β is functionally less relevant than that of tau tangles (Yoshiyama et al., 2013). Nevertheless, we found the highest significant correlations between t-tau/p-tau and FC/EC in sensory and attention related regions in occipital and parietal lobes. It is important to note that CSF biomarker regional correlation patterns do not necessarily correspond to the spatial patterns of amyloid/tau deposition. We speculate that the discrepancy in t-tau/p-tau CSF biomarker regional correlation patterns might indicate a breakdown of sensory integration on the development of cognitive impairments. Finally, APOE4 carriership showed no significant correlations with whole-brain/regional connectivity measures with the exception of left superior frontal EC strength.

This study had several limitations. One limitation rises from the optimization of EC. Given a highly non-linear model, the use of well-established techniques such as Bayesian inference is computationally infeasible. Heuristic approaches to infer EC are difficult to validate given the complexity of the model and the available data. We addressed some of these problems by constraining the parameter space to non-zero connections in structural connectivity (SC) and limiting the parameter range. Another limitation is that the model-based estimation of EC can be strongly influenced by the observed data. One approach to characterize the links between brain regions is the anatomical connectivity measures based on DWI. Nevertheless, DWI suffers from systematic biases (Van Essen et al., 2014), which may get aggravated in subjects with significant neurodegeneration as in AD. Indeed, DWI-
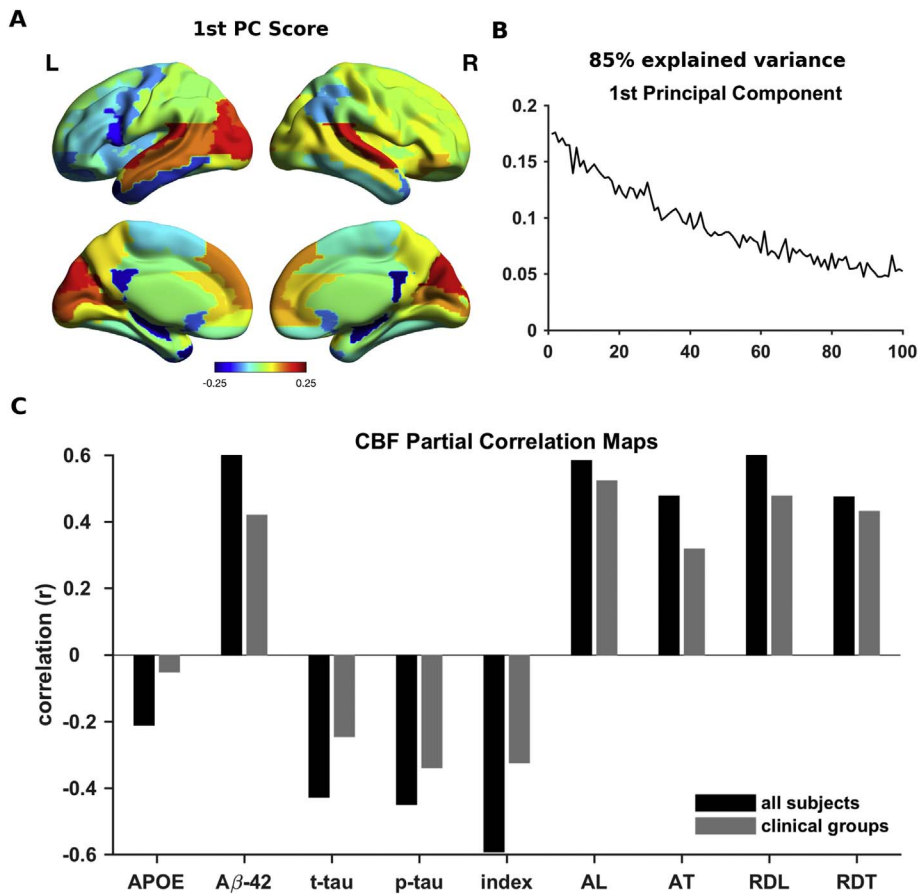
A

1st PC Score

L   R

B

85% explained variance
1st Principal Component

C

CBF Partial Correlation Maps

Fig. 7. Principal Component Analysis (PCA) of the simulated FC strengths across manipulated local bifurcation parameters. A The spatial map of the first principal component scores. The spatial map indicates the most and the least affected regions due to local bifurcation parameter manipulation in hot and cold colors, respectively. B The first principal component reflecting the FC alterations due to the divergence from optimal bifurcation parameter, explaining 85% of the total variance. C The correlation coefficient between the spatial map of first principal component and that of the relationship between FC strength and APOE-4 allelle carier status, CSF biomarkers and behavioral performance measures (i.e. partial correlation coefficients between FC strength and each measure). Black and gray bars indicate across all subject and across clinical group spatial maps, respectively.

based structural connectivity measures performed considerably worse (Supplementary Fig. 8). Furthermore, directed connectivity between cortical areas were shown to be abundant in primates (Markov et al., 2014), which cannot be captured by DWI. We found that the altered patterns of directed EC provided additional information regarding clinical groups including impaired prefrontal input strengths in PAD and MCI groups (Supplementary Figs. 5–7). However, we kept these results out of scope in this study as comprehensive theoretical analysis of the computational model is necessary to understand the role of directed connectivity.

This study showed that whole-brain connectivity alterations in AD progression involve gradual attenuation of overall synchronization primarily affecting the strongly connected brain networks such as DMN. The proposed computational modeling approach revealed that these alterations can be explained by disruptions in local dynamics and the underlying core connectivity changes might be distinct from those observed in FC. The results of this study provide insights to understand functional mechanisms of the progression of symptoms in AD.

Acknowledgements

Appendix A. Supplementary data

Supplementary data to this article can be found online at http://dx.doi.org/10.1016/j.nicl.2017.08.006.

References

Agosta, Federica, Pievani, Michela, Geroldi, Cristina, Copetti, Massimiliano, Frisoni, Giovanni B., Filippi, Massimo, 2012. Resting state fMRI in Alzheimer's disease: beyond the default mode network. Neurobiol. Aging 33 (8), 1564–1578. http://dx.doi.org/10.1016/j.neurobiolaging.2011.06.007.

Allen, Greg, Barnard, Holly, McColl, Roderick, Hester, Andrea L., Fields, Julie A., Weiner, Myron F., Wendy K. Ringe, et al., 2007. Reduced hippocampal functional connectivity in Alzheimer disease. Arch. Neurol. 64 (10), 1482–1487. http://dx.doi.org/10.1001/archneur.64.10.1482.

Ashburner, J., Friston, K.J., 2000. Voxel-based morphometry–the methods. NeuroImage 11 (6 Pt 1), 805–821. http://dx.doi.org/10.1006/nimg.2000.0582.

Avants, Brian B., Tustison, Nicholas J., Song, Gang, Cook, Philip A., Klein, Arno, Gee, James C., 2011. A reproducible evaluation of ANTs similarity metric performance in brain image registration. NeuroImage 54 (3), 2033–2044. http://dx.doi.org/10.1016/j.neuroimage.2010.09.025.

Bai, Jane P.F., Bell, Robert, Buckman, ShaAvhree, Burckart, Gilbert J., Eichler, Hans-Georg, Fang, Kenneth C., Goodsaid, Federico M., et al., 2011. Translational biomarkers: from preclinical to clinical a report of 2009 AAPS/ACCP biomarker workshop. AAPS J. 13 (2), 274–283. http://dx.doi.org/10.1208/s12248-011-9265-x.

Barkhof, Frederik, Haller, Sven, Rombouts, Serge A.R.B., 2014. Resting-state functional MR imaging: a new window to the brain. Radiology 272 (1), 29–49. http://dx.doi.org/10.1148/radiol.14132388.

Blennow, Kaj, de Leon, Mony J., Zetterberg, Henrik, 2006. Alzheimer's disease. Lancet (London, England) 368 (9533), 387–403. http://dx.doi.org/10.1016/S0140-6736(06)69113-7.

Brier, Matthew R., Thomas, Jewell B., Ances, Beau M., 2014. Network dysfunction in Alzheimer's disease: refining the disconnection hypothesis. Brain Connect. 4 (5), 299–311. http://dx.doi.org/10.1089/brain.2014.0236.

Brier, M.R., Gordon, B., Friedrichsen, K., McCarthy, J., Stern, A., Christensen, J., Owen, C., et al., 2016. Tau and A imaging, CSF measures, and cognition in Alzheimers disease. Sci. Transl. Med. 8 (338), 338ra66. http://dx.doi.org/10.1126/scitranslmed.aaf2362.

Broyd, Samantha J., Demanuele, Charmaine, Debener, Stefan, Helps, Suzannah K., James, Christopher J., Sonuga-Barke, Edmund J.S., 2009. Default-mode brain dysfunction in mental disorders: a systematic review. Neurosci. Biobehav. Rev. 33 (3), 279–296. http://dx.doi.org/10.1016/j.neubiorev.2008.09.002.

Buckner, Randy L., Andrews-Hanna, Jessica R., Schacter, Daniel L., 2008. The brain's default network: anatomy, function, and relevance to disease. Ann. N. Y. Acad. Sci. 1124 (March), 1–38. http://dx.doi.org/10.1196/annals.1440.011.

Cabral, Joana, Hugues, Etienne, Kringelbach, Morten L., Deco, Gustavo, 2012. Modeling

the outcome of structural disconnection on resting-state functional connectivity. NeuroImage 62 (3), 1342–1353. http://dx.doi.org/10.1016/j.neuroimage.2012.06.007.

Celone, Kim A., Calhoun, Vince D., Dickerson, Bradford C., Atri, Alireza, Chua, Elizabeth F., Miller, Saul L., DePeau, Kristina, et al., 2006. Alterations in memory networks in mild cognitive impairment and Alzheimer's disease: an independent component analysis. J. Neurosci. Off. J. Soc. Neurosci. 26 (40), 10222–10231. http://dx.doi.org/10.1523/JNEUROSCI.2250-06.2006.

Cole, Michael W., Pathak, Sudhir, Schneider, Walter, 2010. Identifying the Brain's most globally connected regions. NeuroImage 49 (4), 3132–3148. http://dx.doi.org/10.1016/j.neuroimage.2009.11.001.

Córdova-Palomera, Aldo, Kaufmann, Tobias, Persson, Karin, Alnæs, Dag, Doan, Nhat Trung, Moberget, Torgeir, Lund, Martina Jonette, et al., 2017. Disrupted global metastability and static and dynamic brain connectivity across individuals in the Alzheimer's disease continuum. Sci Rep 7 (January), 40268. http://dx.doi.org/10.1038/srep40268.

Coupe, P., Yger, P., Prima, S., Hellier, P., Kervrann, C., Barillot, C., 2008. An optimized blockwise nonlocal means denoising filter for 3-D magnetic resonance images. IEEE Trans. Med. Imaging 27 (4), 425–441. http://dx.doi.org/10.1109/TMI.2007.906087.

Deco, Gustavo, Kringelbach, Morten L., 2014. Great expectations: using whole-brain computational connectomics for understanding neuropsychiatric disorders. Neuron 84 (5), 892–905. http://dx.doi.org/10.1016/j.neuron.2014.08.034.

Deco, Gustavo, Kringelbach, Morten L., Jirsa, Viktor K., Ritter, Petra, 2017. The dynamics of resting fluctuations in the brain: metastability and its dynamical cortical core. Sci Rep 7 (1). http://dx.doi.org/10.1038/s41598-017-03073-5.

Dennis, Emily L., Thompson, Paul M., 2014. Functional brain connectivity using fMRI in aging and Alzheimer's disease. Neuropsychol. Rev. 24 (1), 49–62. http://dx.doi.org/10.1007/s11065-014-9249-6.

Dickerson, Bradford C., Salat, David H., Bates, Julianna F., Atiya, Monika, Killiany, Ronald J., Greve, Douglas N., Anders M. Dale, et al., 2004. Medial temporal lobe function and structure in mild cognitive impairment. Ann. Neurol. 56 (1), 27–35. http://dx.doi.org/10.1002/ana.20163.

Essen, Van, David, C., Jbabdi, Saad, Sotiropoulos, Stamatios N., Chen, Charles, Dikranian, Krikor, Coalson, Tim, Harwell, John, Behrens, Timothy E.J., Glasser, Matthew F., 2014. Mapping connections in humans and non-human primates: aspirations and challenges for diffusion imaging. In: Diffusion MRI, Second Edition. Academic Press, San Diego, pp. 337–358. http://www.sciencedirect.com/science/article/pii/B9780123964601000160.

Filippi, Massimo, Agosta, Federica, 2011. Structural and functional network connectivity breakdown in Alzheimer's disease studied with magnetic resonance imaging techniques. J. Alzheimers Dis. 24 (3), 455–474. http://dx.doi.org/10.3233/JAD-2011-101854.

Friston, K.J., Harrison, L., Penny, W., 2003. Dynamic causal modelling. NeuroImage 19 (4), 1273–1302.

Glerean, Enrico, Salmi, Juha, Lahnakoski, Juha M., Jaaskelainen, Iiro P., Sams, Mikko, 2012. Functional magnetic resonance imaging phase synchronization as a measure of dynamic functional connectivity. Brain Connect. 2 (2), 91–101. http://dx.doi.org/10.1089/brain.2011.0068.

Greicius, Michael, 2008. Resting-state functional connectivity in neuropsychiatric disorders. Curr. Opin. Neurol. 21 (4), 424–430. http://dx.doi.org/10.1097/WCO.0b013e328306f2c5.

Greicius, Michael D., Srivastava, Gaurav, Reiss, Allan L., Menon, Vinod, 2004. Default-mode network activity distinguishes Alzheimer's disease from healthy aging: evidence from functional MRI. Proc. Natl. Acad. Sci. U. S. A. 101 (13), 4637–4642. http://dx.doi.org/10.1073/pnas.0308627101.

Hagmann, Patric, Cammoun, Leila, Gigandet, Xavier, Meuli, Reto, Honey, Christopher J., Wedeen, Van J., Sporns, Olaf, 2008. Mapping the structural core of human cerebral cortex. PLoS Biol. 6 (7), e159. http://dx.doi.org/10.1371/journal.pbio.0060159.

Hedden, Trey, Van Dijk, Koene R.A., Alex Becker, J., Mehta, Angel, Sperling, Reisa A., Johnson, Keith A., Buckner, Randy L., 2009. Disruption of functional connectivity in clinically normal older adults harboring amyloid burden. J. Neurosci. Off. J. Soc. Neurosci. 29 (40), 12686–12694. http://dx.doi.org/10.1523/JNEUROSCI.3189-09.2009.

Hellyer, Peter J., Shanahan, Murray, Scott, Gregory, Wise, Richard J.S., Sharp, David J., Leech, Robert, 2014. The control of global brain dynamics: opposing actions of frontoparietal control and default mode networks on attention. J. Neurosci. 34 (2), 451–461. http://dx.doi.org/10.1523/JNEUROSCI.1853-13.2014.

Hochberg, Yosef, Benjamini, Yoav, 1990. More powerful procedures for multiple significance testing. Stat. Med. 9 (7), 811–818. http://dx.doi.org/10.1002/sim.4780090710.

Jack, Clifford R., Albert, Marilyn, Knopman, David S., McKhann, Guy M., Sperling, Reisa A., Carillo, Maria, Thies, William, Phelps, Creighton H., 2011. Introduction to revised criteria for the diagnosis of Alzheimer's disease: National Institute on Aging and the Alzheimer Association Workgroups. Alzheimers Dement. 7 (3), 257–262. http://dx.doi.org/10.1016/j.jalz.2011.03.004.

Jenkinson, Mark, Beckmann, Christian F., Behrens, Timothy E.J., Woolrich, Mark W., Smith, Stephen M., 2012. FSL. NeuroImage 62 (2), 782–790. http://dx.doi.org/10.1016/j.neuroimage.2011.09.015.

Koch, W., Teipel, S., Mueller, S., Buerger, K., Bokde, A.L.W., Hampel, H., Coates, U., Reiser, M., Meindl, T., 2010. Effects of aging on default mode network activity in resting state fMRI: does the method of analysis matter? NeuroImage 51 (1), 280–287. http://dx.doi.org/10.1016/j.neuroimage.2009.12.008.

Kuramoto, Y., 1986. Chemical Oscillations, Waves, and Turbulence. 66 (7). Springer-Verlag, Berlin-Heidelberg-New York-Tokyo, pp. 296. http://dx.doi.org/10.1002/zamm.19860660706.

Lemieux, Louis, Salek-Haddadi, Afraim, Lund, Torben E., Laufs, Helmut, Carmichael,

David, 2007. Modelling large motion events in fMRI studies of patients with epilepsy. Magn. Reson. Imaging 25 (6), 894–901. http://dx.doi.org/10.1016/j.mri.2007.03.009.

Li, Wenjun, Antuono, Piero G., Xie, Chunming, Chen, Gang, Jones, Jennifer L., Douglas Ward, B., Franczak, Malgorzata B., Goveas, Joseph S., Li, Shi-Jiang, 2012. Changes in regional cerebral blood flow and functional connectivity in the cholinergic pathway associated with cognitive performance in subjects with mild Alzheimer's disease after 12-week donepezil treatment. NeuroImage 60 (2), 1083–1091. http://dx.doi.org/10.1016/j.neuroimage.2011.12.077.

Li, Xiaozhen, Li, Tie-Qiang, Andreasen, Niels, Wiberg, Maria Kristoffersen, Westman, Eric, Wahlund, Lars-Olof, 2013. Ratio of Aβ42/P-tau181p in CSF is associated with aberrant default mode network in AD. Sci Rep 3 (February). http://dx.doi.org/10.1038/srep01339.

Lustig, Cindy, Snyder, Abraham Z., Bhakta, Mehul, O'Brien, Katherine C., McAvoy, Mark, Raichle, Marcus E., Morris, John C., Buckner, Randy L., 2003. Functional deactivations: change with age and dementia of the Alzheimer type. Proc. Natl. Acad. Sci. U. S. A. 100 (24), 14504–14509. http://dx.doi.org/10.1073/pnas.2235925100.

Manjón, José V., Coupé, Pierrick, Concha, Luis, Antonio, Buades, Louis Collins, D., Robles, Montserrat, 2013. Diffusion weighted image denoising using overcomplete local PCA. PLoS One 8 (9), e73021. http://dx.doi.org/10.1371/journal.pone.0073021.

Margulies, Daniel S., Ghosh, Satrajit S., Goulas, Alexandros, Falkiewicz, Marcel, Huntenburg, Julia M., Langs, Georg, Bezgin, Gleb, et al., 2016. Situating the default-mode network along a principal gradient of macroscale cortical organization. Proc. Natl. Acad. Sci. 113 (44), 12574–12579. http://dx.doi.org/10.1073/pnas.1608282113.

Markov, N.T., Ercsey-Ravasz, M.M., Ribeiro Gomes, A.R., Lamy, C., Magrou, L., Vezoli, J., Misery, P., et al., 2014. A weighted and directed interareal connectivity matrix for macaque cerebral cortex. Cereb. Cortex 24 (1), 17–36. http://dx.doi.org/10.1093/cercor/bhs270.

Molinuevo, Jose Luis, Domingo, Gispert Juan, Bruno, Dubois, Heneka, Michael T., Alberto, Lleo, Sebastiaan, Engelborghs, Jesús, Pujol, et al., 2013. The AD-CSF-index discriminates Alzheimer's disease patients from healthy controls: a validation study. J. Alzheimers Dis. 1, 67–77. http://dx.doi.org/10.3233/JAD-130203.

Molinuevo, José Luis, Blennow, Kaj, Dubois, Bruno, Engelborghs, Sebastiaan, Lewczuk, Piotr, Perret-Liaudet, Armand, Teunissen, Charlotte E., Parnetti, Lucilla, 2014. The clinical use of cerebrospinal fluid biomarker testing for Alzheimer's disease diagnosis: a consensus paper from the Alzheimer's biomarkers standardization initiative. Alzheimers Dement. 10 (6), 808–817. http://dx.doi.org/10.1016/j.jalz.2014.03.003.

Murphy, Kevin, Birn, Rasmus M., Handwerker, Daniel A., Jones, Tyler B., Bandettini, Peter A., 2009. The impact of global signal regression on resting state correlations: are anti-correlated networks introduced? NeuroImage 44 (3), 893–905. http://dx.doi.org/10.1016/j.neuroimage.2008.09.036.

Musiek, Erik S., Holtzman, David M., 2015. Three dimensions of the amyloid hypothesis: time, space and 'wingmen'. Nat. Neurosci. May, 800–806. http://dx.doi.org/10.1038/nn.4018.

Oh, Hwamee, Mormino, Elizabeth C., Madison, Cindee, Hayenga, Amynta, Smiljic, Andre, Jagust, William J., 2011. β-Amyloid affects frontal and posterior brain networks in normal aging. NeuroImage 54 (3), 1887–1895. http://dx.doi.org/10.1016/j.neuroimage.2010.10.027.

Palop, Jorge J., Mucke, Lennart, 2016. Network abnormalities and interneuron dysfunction in Alzheimer disease. Nat. Rev. Neurosci. 17 (12), 777–792. http://dx.doi.org/10.1038/nrn.2016.141.

Petrella, Jeffrey R., Wang, Lihong, Krishnan, Sriyesh, Slavin, Melissa J., Prince, Steven E., Tran, Thanh-Thu T., Murali Doraiswamy, P., 2007. Cortical deactivation in mild cognitive impairment: high-field-strength functional MR imaging. Radiology 245 (1), 224–235. http://dx.doi.org/10.1148/radiol.2451061847.

Pike, K.E., Savage, G., Villemagne, V.L., Ng, S., Moss, S.A., Maruff, P., Mathis, C.A., Klunk, W.E., Masters, C.L., Rowe, C.C., 2007. β-Amyloid imaging and memory in non-demented individuals: evidence for preclinical Alzheimer's disease. Brain 130 (11), 2837–2844. http://dx.doi.org/10.1093/brain/awm238.

Plassman, B.L., Langa, K.M., Fisher, G.G., Heeringa, S.G., Weir, D.R., Ofstedal, M.B., Burke, J.R., et al., 2007. Prevalence of dementia in the United States: the aging, demographics, and memory study. Neuroepidemiology 29 (1–2), 125–132. http://dx.doi.org/10.1159/000109998.

Price, J.L., Morris, J.C., 1999. Tangles and plaques in nondemented aging and 'preclinical' Alzheimer's disease. Ann. Neurol. 45 (3), 358–368.

Qi, Zhigang, Wu, Xia, Wang, Zhiqun, Zhang, Nang, Dong, Huiqing, Yao, Li, Li, Kuncheng, 2010. Impairment and compensation coexist in amnestic MCI default mode network. NeuroImage 50 (1), 48–55. http://dx.doi.org/10.1016/j.neuroimage.2009.12.025.

Ramirez, Maria J., Lai, Mitchell K.P., Tordera, Rosa M., Francis, Paul T., 2014. Serotonergic therapies for cognitive symptoms in Alzheimer's disease: rationale and current status. Drugs 74 (7), 729–736. http://dx.doi.org/10.1007/s40265-014-0217-5.

Rogers, Baxter P., Katwal, Santosh B., Morgan, Victoria L., Asplund, Christopher L., Gore, John C., 2010. Functional MRI and multivariate autoregressive models. Magn. Reson. Imaging 28 (8), 1058–1065. http://dx.doi.org/10.1016/j.mri.2010.03.002.

Rombouts, Serge A.R.B., Barkhof, Frederik, Goekoop, Rutger, Stam, Cornelis J., Scheltens, Philip, 2005. Altered resting state networks in mild cognitive impairment and mild Alzheimer's disease: an fMRI study. Hum. Brain Mapp. 26 (4), 231–239. http://dx.doi.org/10.1002/hbm.20160.

Rombouts, Serge A.R.B., Damoiseaux, Jessica S., Goekoop, Rutger, Barkhof, Frederik, Scheltens, Philip, Smith, Stephen M., Beckmann, Christian F., 2009. Model-free group analysis shows altered BOLD FMRI networks in dementia. Hum. Brain Mapp. 30 (1), 256–266. http://dx.doi.org/10.1002/hbm.20505.

Sanz-Arigita, Ernesto J., Schoonheim, Menno M., Damoiseaux, Jessica S., Rombouts,

Serge A.R.B., Maris, Erik, Barkhof, Frederik, Scheltens, Philip, Stam, Cornelis J., 2010. Loss of 'small-world' networks in Alzheimer's disease: graph analysis of FMRI resting-state functional connectivity. PLoS One 5 (11), e13788. http://dx.doi.org/10.1371/journal.pone.0013788.

Shanahan, Murray, 2010. Metastable chimera states in community-structured oscillator networks. Chaos (Woodbury, N.Y.) 20 (1), 13108. http://dx.doi.org/10.1063/1.3305451.

Sheline, Yvette I., Raichle, Marcus E., 2013. Resting state functional connectivity in preclinical Alzheimer's disease. Biol. Psychiatry 74 (5), 340–347. http://dx.doi.org/10.1016/j.biopsych.2012.11.028.

Sheline, Yvette I., Morris, John C., Snyder, Abraham Z., Price, Joseph L., Yan, Zhizi, D'Angelo, Gina, Liu, Collin, et al., 2010a. APOE4 allele disrupts resting state fMRI connectivity in the absence of amyloid plaques or decreased CSF Aβ42. J. Neurosci. 30 (50), 17035–17040. http://dx.doi.org/10.1523/JNEUROSCI.3987-10.2010.

Sheline, Yvette I., Raichle, Marcus E., Snyder, Abraham Z., Morris, John C., Head, Denise, Wang, Suzhi, Mintun, Mark A., 2010b. Amyloid plaques disrupt resting state default mode network connectivity in cognitively normal elderly. Biol. Psychiatry 67 (6), 584–587. http://dx.doi.org/10.1016/j.biopsych.2009.08.024.

Singh, V., Chertkow, H., Lerch, J.P., Evans, A.C., Dorr, A.E., Kabani, N.J., 2006. Spatial patterns of cortical thinning in mild cognitive impairment and Alzheimer's disease. Brain 129 (11), 2885–2893. http://dx.doi.org/10.1093/brain/awl256.

Sorg, Christian, Riedl, Valentin, Mühlau, Mark, Calhoun, Vince D., Eichele, Tom, Läer, Leonhard, Drzezga, Alexander, et al., 2007. Selective changes of resting-state networks in individuals at risk for Alzheimer's disease. Proc. Natl. Acad. Sci. U. S. A. 104 (47), 18760–18765. http://dx.doi.org/10.1073/pnas.0708803104.

Sperling, Reisa A., Laviolette, Peter S., O'Keefe, Kelly, O'Brien, Jacqueline, Rentz, Dorene M., Pihlajamaki, Maija, Marshall, Gad, et al., 2009. Amyloid deposition is associated with impaired default network function in older persons without dementia. Neuron 63 (2), 178–188. http://dx.doi.org/10.1016/j.neuron.2009.07.003.

Thompson, Paul M., Hayashi, Kiralee M., de Zubicaray, Greig, Janke, Andrew L., Rose, Stephen E., Semple, James, Herman, David, et al., 2003. Dynamics of gray matter loss in Alzheimer's disease. J. Neurosci. 23 (3), 994.

Tustison, Nicholas J., Avants, Brian B., Cook, Philip A., Zheng, Yuanjie, Egan, Alexander, Yushkevich, Paul A., Gee, James C., 2010. N4ITK: improved N3 bias correction. IEEE Trans. Med. Imaging 29 (6), 1310–1320. http://dx.doi.org/10.1109/TMI.2010.2046908.

Tzourio-Mazoyer, N., Landeau, B., Papathanassiou, D., Crivello, F., Etard, O., Delcroix, N., Mazoyer, B., Joliot, M., 2002. Automated anatomical labeling of activations in SPM using a macroscopic anatomical parcellation of the MNI MRI single-subject brain. NeuroImage 15 (1), 273–289. http://dx.doi.org/10.1006/nimg.2001.0978.

Wang, Liang, Zang, Yufeng, He, Yong, Liang, Meng, Zhang, Xinqing, Tian, Lixia, Wu, Tao, Jiang, Tianzi, Li, Kuncheng, 2006. Changes in hippocampal connectivity in the early stages of Alzheimer's disease: evidence from resting state fMRI. NeuroImage 31 (2), 496–504. http://dx.doi.org/10.1016/j.neuroimage.2005.12.033.

Wang, Liang, Brier, Matthew R., Snyder, Abraham Z., Thomas, Jewell B., Fagan, Anne M., Xiong, Chengjie, Benzinger, Tammie L., Holtzman, David M., Morris, John C., Ances, Beau M., 2013. Cerebrospinal fluid Aβ42, phosphorylated Tau181, and resting-state functional connectivity. JAMA Neurol. 70 (10), 1242–1248. http://dx.doi.org/10.1001/jamaneurol.2013.3253.

Wee, Chong-Yaw, Yap, Pew-Thian, Denny, Kevin, Browndyke, Jeffrey N., Potter, Guy G., Welsh-Bohmer, Kathleen A., Wang, Lihong, Shen, Dinggang, 2012. Resting-state multi-spectrum functional connectivity networks for identification of MCI patients. PLoS One 7 (5). http://dx.doi.org/10.1371/journal.pone.0037828.

Xia, Mingrui, Wang, Jinhui, He, Yong, 2013. BrainNet viewer: a network visualization tool for human brain connectomics. PLoS One 8 (7), e68910. http://dx.doi.org/10.1371/journal.pone.0068910.

Yang, Genevieve J., Murray, John D., Repovs, Grega, Cole, Michael W., Savic, Aleksandar, Glasser, Matthew F., Pittenger, Christopher, et al., 2014. Altered global brain signal in schizophrenia. Proc. Natl. Acad. Sci. U. S. A. 111 (20), 7438–7443. http://dx.doi.org/10.1073/pnas.1405289111.

Yoshiyama, Yasumasa, Lee, Virginia M.Y., Trojanowski, John Q., 2013. Therapeutic strategies for tau mediated neurodegeneration. J. Neurol. Neurosurg. Psychiatry 84 (7), 784–795. http://dx.doi.org/10.1136/jnnp-2012-303144.

Zhang, Hong-Ying, Wang, Shi-Jie, Xing, Jiong, Liu, Bin, Ma, Zhan-Long, Yang, Ming, Zhang, Zhi-Jun, Teng, Gao-Jun, 2009. Detection of PCC functional connectivity characteristics in resting-state fMRI in mild Alzheimer's disease. Behav. Brain Res. 197 (1), 103–108. http://dx.doi.org/10.1016/j.bbr.2008.08.012.